Biol. Cybern. 72, 475–485 (1995)

Biological Cybernetics

Human hand impedance characteristics during maintained posture

Toshio Tsuji[1], Pietro G. Morasso[2], Kazuhiro Goto[1], Koji Ito[3]

[1] Faculty of Engineering, Hiroshima University, 4-1, Kagamiyama 1-chome, Higashi-Hiroshima, 724 Japan
[2] Department of Informatics, Systems and Telecommunications, University of Genova, Via Opera Pia 11A, I-16145 Genova, Italy
[3] Toyohashi University of Technology, 1-1, Hibarigaoka, Tenpaku-cho, Toyohashi, 400 Japan
Bio-mimetic Control Research Center, Rikon, 3-8-31, Rokuban, Atsuta-ku, Nagoya, 456 Japan

Received: 23 June 1993 / Accepted in revised form: 15 September 1994

Abstract. The present paper examines human hand impedance characteristics, including inertia and viscosity as well as stiffness, in multi-joint arm movements. While a subject maintains a given hand location, small external disturbances are applied to his hand by a manipulandum. The corresponding force-displacement vectors are measured and sampled over time in order to estimate the hand impedance by means of a second-order linear model. The experimental results in different subjects and hand locations are summarized as follows: (1) the estimated inertia matrices of the human hand well agrees with computed values using a two-joint arm model, (2) spatial variations of the stiffness ellipses are consistent with the experimental results of Mussa-Ivaldi et al. (1985), (3) hand stiffness and viscosity increase with the grip force of the subject, and (4) viscosity and stiffness ellipses tend to have similar orientation. The accuracy of the impedance estimation method is validated with a mechanical spring-mass system with known parameters.

1 Introduction

Our goal in the present paper is to find hand impedance characteristics including stiffness, viscosity and inertia in multi-joint arm movements. In previous studies of human arm movement control, Bizzi et al. (1984) showed that the arm of a deafferented monkey returned toward an intermediate position between the initial and target positions when the arm was moved toward the target position before onset of the arm movement in such a way that the monkey could not detect it. The experimental results mean that the central nervous system plans not only the final equilibrium position but also a time series of equilibrium points of the arm movement. Hogan (1984) named the time series of equilibrium points a virtual trajectory and proposed a consequent control hypothesis which assumes that the actual arm trajectory is produced by the gradual shift of the hand equilibrium position and impedance determined by muscular viscoelastic properties. Flash (1987) performed computer simulations of a two-joint planar arm based on the virtual trajectory control hypothesis and showed that simulated results using straight virtual trajectories determined by a minimum jerk criterion agreed well with measured trajectories of human arms, thus suggesting that the central nervous system could control arm movements through the equilibrium trajectories and the viscoelastic properties of the musculoskeletal system without solving the inverse dynamic problem of the multi-joint arm explicitly.

The other approach to explain the feedforward control of voluntary movements is based on internal models of motor control systems which are acquired through biological motor learning. Kawato et al. (1987) proposed a hierarchical neural network model which can solve both the inverse kinematic and the inverse dynamic problems by using a feedback error learning scheme. Then, Katayama and Kawato (1991a) proposed a parallel hierarchical neural network model which includes inverse static and dynamic models. The inverse static model mainly controls the equilibrium posture and the arm stiffness, and the inverse dynamic model plays a role in compensating the non-linear dynamics of the arm during fast movements. They found through computer simulations using a two-joint and six-muscle arm model that the virtual trajectories learned during fast movements largely differed from the actual arm trajectories (Katayama and Kawato 1991b, 1993).

In both motor control schemes, the viscoelastic properties of the musculoskeletal system play an important role. In computer simulations of two-joint arms by Flash (1987) and Katayama and Kawato (1991a, b, 1993), for example, different values of the viscoelastic coefficients of joints or muscles may determine quite different simulation results. In order to validate such simulation studies of multi-joint arm movements, it is necessary to rely on precise estimates of the viscoelastic property of the musculoskeletal system.

Several studies have been made for single-joint arm movements. Especially in terms of impedance characteristics of the elbow joint, it has been shown that viscoelastic coefficients change depending on the activation level of muscles (Cannon and Zahalak 1982), task instruction to the subjects (Lacquaniti et al. 1982), joint angles (MacKay et

Correspondence to: T. Tsuji (Tel:+81-824-24-7692, Fax:+81-824-22-7195
E-mail tsuji@huis.hiroshima-u.ac.jp)

al. 1986), presence or absence of dynamic arm movements (Bennett et al. 1992), and speed of arm movement and loading (Milner 1993). Unfortunately, impedance properties during multi-joint arm movements cannot be predicted from experimental results with single-joint arm movements because of viscoelastic properties of the shoulder joint and interactions between joints caused by multi-joint muscles.

For the multi-joint arm movements, however, only two kinds of experiments have been reported so far:[1] arm stiffness during posture (Mussa-Ivaldi et al. 1985 and Flash and Mussa- Ivaldi 1990) and during dynamic arm movements (Gomi et al. 1992a, b).

Mussa-Ivaldi et al. (1985) developed an experimental method to measure human hand stiffness while maintaining posture. The hand of the subject was displaced from an equilibrium position by a two-joint manipulandum and then the restoring forces were measured at steady state (from 0.6 s to 1.1 s after the onset of the external disturbance). The hand stiffness characteristics computed from the displacements and forces indicated that the hand stiffness systematically depended on the hand locations and arm postures in the horizontal plane, and that the subjects could not regulate the orientations and shapes of the stiffness ellipses. Flash and Mussa-Ivaldi (1990) showed that the spatial variations of the hand stiffness ellipses in the horizontal plane could be explained by a covariation between the shoulder stiffness and the stiffness component provided by two-joint muscles. Gomi et al. (1992a, b) estimated hand stiffness along one direction in the horizontal plane during two-joint arm movements and argued that dynamic stiffness might be lower than the static one.

In any case, previous investigators estimated only the hand stiffness of the multi-joint arm movements and did not consider the global impedance which includes inertia and viscosity characteristics as well. In particular, the role of the hand viscosity characteristics in multi-joint arm movements should be made clear in terms of relations to hand stiffness, since the viscous property of skeletal muscles largely changes depending on their activation levels, just like muscle stiffness.

In this paper, the estimation method developed by Mussa-Ivaldi et al. (1985) is extended to estimate the human hand inertia and viscosity as well as stiffness in the multi-joint arm movements. While a subject maintains a given hand location, small external disturbances to the hand are applied by a manipulandum. Time changes of the hand displacements and forces caused by the disturbances are measured, and the hand impedance is estimated using a second-order linear model. In addition, the accuracy of the estimation method was first tested by applying it to a mechanical system with known parameters.

2 Methods

2.1 Hand impedance model

The following hand impedance model is assumed:

[1] Recently, Dolan et al. (1993) also extended the experimental method developed by Mussa-Ivaldi et al. (1985) to include measurement of dynamic components such as viscosity and inertia as well as stiffness

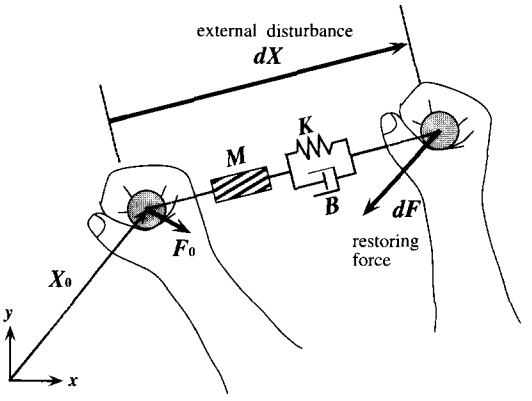

Fig. 1. Description of hand impedance for small motions around an equilibrium posture. While the subject maintains a hand location, a small external disturbance to the hand is applied by a manipulandum. Time changes of the hand displacements and forces caused by the disturbance are measured, and the hand impedance is estimated using a second-order linear model

$$\mathbf{M}(t)\ddot{X}(t) + \mathbf{B}(t)\dot{\mathbf{X}}(t) + \mathbf{K}(t)(X(t) - X_\nu(t)) = -F(t) \qquad (1)$$

where $X(t) \in R^l$ is the hand position vector; $F(t) \in R^l$ is the force vector exerted by the hand to the environment; $X(t) \in R^l$ represents a virtual equilibrium point (or a virtual trajectory); $\mathbf{M}(t)$,$\mathbf{B}(t)$ and $\mathbf{K}(t) \in R^{l\times l}$ represent hand inertia, viscosity and stiffness matrices, respectively; and l is the dimensionality of the task space. $\mathbf{M}(t)$ is the equivalent inertia evaluated in the task space and is known to be strongly dependent upon arm postures (Asada and Slotine 1986). The hand viscosity $\mathbf{B}(t)$ and hand stiffness $\mathbf{K}(t)$ also depend on the viscoelastic properties of skeletal muscles, low- level neural reflexes and passive elements such as skins and veins.

In order to estimate its impedance, the hand of the subject is displaced from an equilibrium by means of a small disturbance of short duration (Fig.1). The small size of the disturbance is necessary in order to assume the approximate constancy of $\mathbf{M}, \mathbf{B}$ and $\mathbf{K}$, which are known to depend on posture only in a smooth way. The short duration of the disturbance is demanded by the need to avoid a variation of the virtual equilibrium point X_v during the measurement due to voluntary neural feedback. As a result, hand inertia, viscosity, stiffness and the virtual equilibrium point are assumed to be constant after the onset of the disturbance. Then we can limit ourselves to a constant parameter, second-order, linear impedance model of the hand dynamics for small motions around an equilibrium posture:

$$\mathbf{M}\ddot{X}(t) + \mathbf{B}\dot{X}(t) + \mathbf{K}(X(t) - X_\nu) = -F(t) \qquad (2)$$

Moreover, since at the onset time t_0 of the disturbance we have

$$\mathbf{M}\ddot{X}(t_0) + \mathbf{B}\dot{X}(t_0) + \mathbf{K}(X(t_0) - X_\nu) = -F(t_0) \qquad (3)$$

we can eliminate $\mathbf{X}_\nu$ from (2) and (3).

$$\mathbf{M}d\ddot{X}(t) + \mathbf{B}d\dot{X}(t) + \mathbf{K}dX(t) = -F(t) \qquad (4)$$

here $dX(t) \equiv X(t) - X(t_0)$ and $dF(t) \equiv F(t) - F(t_0)$. In this equation, $\mathbf{M}, \mathbf{B}$ and $\mathbf{K}$ are unknown parameters and the other either variables are direct measurements [$dX(t)$ and $\mathbf{F}(t)$) or

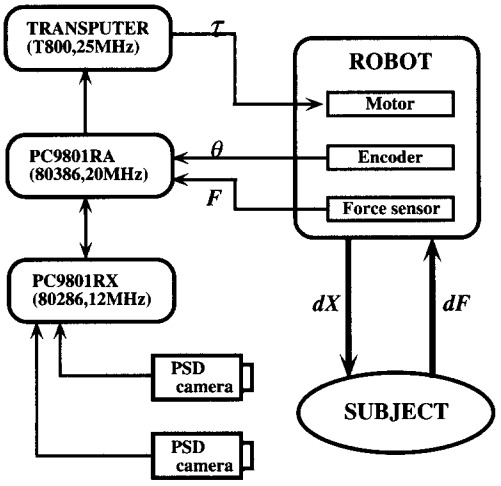

Fig. 2. Experimental apparatus for hand impedance estimation. A two-joint planar direct drive robot was used as a manipulandum. Hand Forces and positions of the subject were measured by a force sensor attached to the robot handle (resolution: 0.05 N for both x axis and y axis) and optical encoders of the robot joints (resolution 1.745×10^{-5} rad), respectively. The arm posture of the subject was measured by a stereo-PSD camera system. The data sampling intervals were 1 ms for hand forces and positions, 10 ms for 3D arm postures and 0.65 ms for the robot controller

derived by numerical methods. Since the equation is linear in the parameters, the estimation problem can be solved by means of the standard least square procedure. However, we applied this procedure not to (4) but to the following one, obtained by integrating twice over time,

$$\mathbf{M}dX + \mathbf{B}\int_{t_0}^{t_f} \mathrm{d}X(t)\mathrm{d}t + \mathbf{K}\int\int_{t_0}^{t_f} \mathrm{d}X(t)\mathrm{d}t^2 = -\int\int_{t_0}^{t_f} \mathrm{d}F(t)\mathrm{d}t^2 \quad (5)$$

because integration is numerically a more robust operator than differentiation. Note that t_f denotes the length of the data observation window.

2.2 Experiments

Figure 2 shows experimental apparatus for hand impedance estimation. A direct drive robot with a two-joint planar structure was used as a manipulandum in order to apply the external displacements to the hand of the subject. A feedback control law in the task space was used for robot control:

$$\tau = \mathbf{J}_D(\mathbf{q})^T(\mathbf{K}_e(X_d - X) - \mathbf{B}_e\dot{X} \quad (6)$$

where τ and $\mathbf{q} \in R^2$ are the joint control torque vector and the joint angle vector, respectively; $\mathbf{J}_D(\mathbf{q}) \in R^{2\times 2}$ is the Jacobian matrix; $\mathbf{K}_e$ and $\mathbf{B}_e \in R^{2\times 2}$ denote the position and velocity feedback gain matrices, respectively; $X = (x, y)^T$ is the position vector of a handle attached to the endpoint of the robot, and $\mathbf{X}_d$ is the desired (disturbance) trajectory. The feedback gain matrices used in the experiments were $\mathbf{K}_e = \mathrm{diag}[1000 \times 9.8\mathrm{N/m}, 1000 \times 9.8\mathrm{N/m}]$ and $\mathbf{B}_e = \mathrm{diag}[8000 \times 9.8\mathrm{Ns/m}, 8000 \times 9.8\mathrm{Ns/m}]$; the sampling

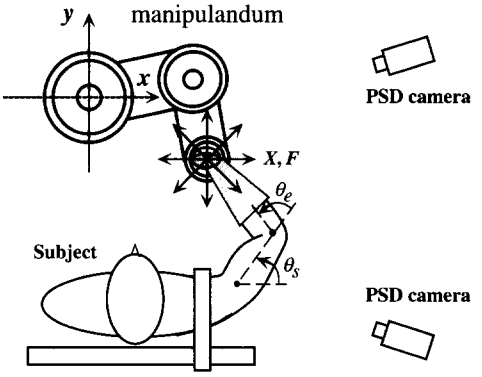

Fig. 3. Subject and manipulandum. The right shoulder of the subject was restrained by a belt to the chair back, and the elbow of the right arm was supported in the horizontal plane by a chain attached to the ceiling. The wrist and the hand were fixed by a molded plastic cast tightly attached to the robot handle

interval of the controller was 0.65 ms. The manipulandum joint angles $\mathbf{q}$ were measured by means of optical encoders (resolution : 1.745×10^{-5} rad), and from this we could compute the Jacobian matrix $\mathbf{J}_D(\mathbf{q})$ and the handle position X by standard kinematic methods (Paul 1981).

The force vector between the hand and the handle was measured by a force sensor attached to the robot handle (resolution : 0.05 N for both x- and y-axes). The arm posture of the subject was measured by a stereo-PSD camera system which was able to compute a three-dimensional (3D) arm posture from the detected positions of four LED targets attached to the shoulder, elbow and wrist joints of the subject and the robot handle. The data sampling intervals were 1 ms for hand forces and positions, and 10 ms for 3D arm postures.

The subject took a seat in the front of the robot (Fig.3), similarly to the experimental method developed by Mussa-Ivaldi et al. (1985). The right shoulder of the subject was restrained by a belt to the chair back, and the elbow of the right arm was supported in the horizontal plane by a chain attached to the ceiling. The wrist and the hand were fixed by a molded plastic cast (mass 0.164 kg) tightly attached to the robot handle in order to eliminate the need for a voluntary grasping action which might influence the measurements of the hand impedance. Moreover, for avoiding voluntary responses of the subject evoked by visual feedback, the robot handle and subject's arm were hidden by a cover in such a way that the subject could not see the robot and arm movements.

The robot was positioned at one of the starting points $\mathbf{X}_0$ using the feedback control law (6). The subject was asked to relax his arm in order to start with a low value of the initial hand force to the handle, and to keep his hand at the initial position. Then an external disturbance was applied to his hand by the robot.

Figure 4 shows the profile of the disturbance pattern, which had an amplitude of about 10 mm and returned to the initial position in about 400 ms. This should eliminate any significant influence of voluntary responses of the subject on the measurements performed. Moreover, in order to avoid prediction by the subject, the time onset of the disturbance and its direction (among eight possible ones, see Fig.3) were

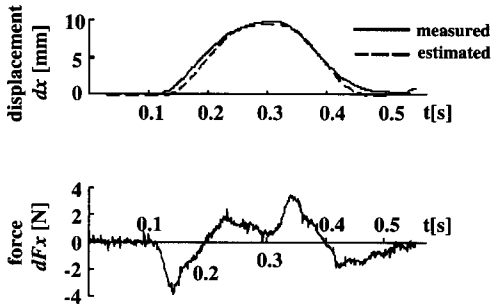

Fig. 4. Example of measured displacement and force profiles purely determined by the mass of the handle. The estimated displacement profile was obtained by numerical integration of (4) for the estimated mass of the handle. Note that the disturbance was applied along the direction of the x-axis

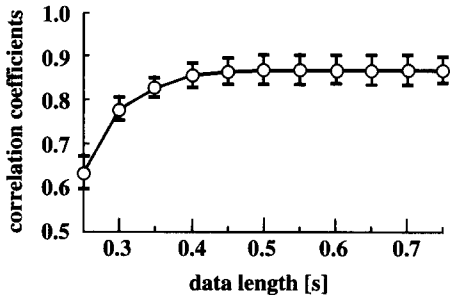

Fig. 5. Correlation coefficients between measured and predicted values of the displacement $d\mathbf{X}(t)$. Mean values and standard deviations for 6 sets of estimated results are plotted, where the *horizontal axis* shows data length used for the least square method. The data length represents the time from the onset of the disturbance (data sampling interval is 1 ms)

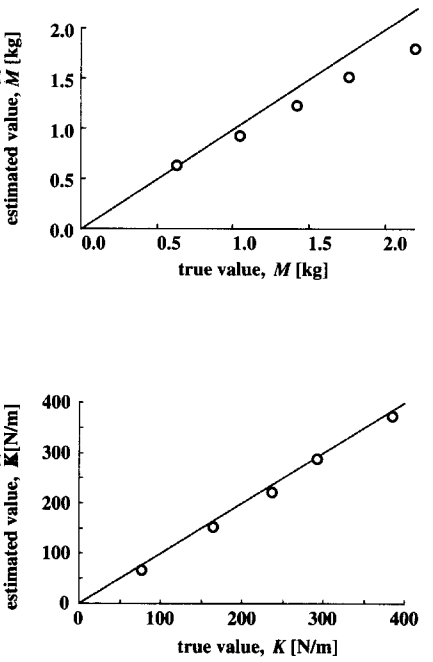

Fig. 6a,b. Accuracy of estimated impedance. The method was applied to the estimation of the mass (i.e. inertia) of brass weights and the spring coefficients (i.e. stiffness) of mechanical springs, where the maximum amplitude of the disturbance was 10 mm and the data length for the least square method was 450 ms. **a** Comparison between true and estimated inertia. Mean values for 6 sets of estimated results are plotted. Note that the SD for each estimated inertia was less than 0.05 kg. **b** Comparison between true and estimated stiffness. Mean values for 6 sets of estimated results are plotted. Note that the SD for each estimated stiffness was less than 5 N/m

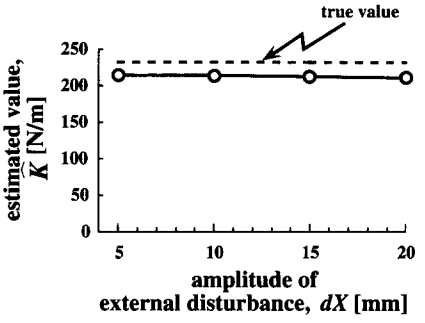

Fig. 7. Effect of disturbance amplitude on estimated stiffness. Mean values for 6 sets of estimated results are plotted. Note that the SD for each estimated stiffness was less than 5 N/m

chosen in a random way. Then the time changes of the hand displacements $dX(t)$ and hand force $dF(t)$ were measured, and the hand impedance, $\mathbf{M}, \mathbf{B}, \mathbf{K}$, were estimated for a set of data corresponding to eight disturbances with different directions. Mean values and standard deviations of the hand impedance for the six data sets were used in the following analysis.

Our experimental approach differs from the one described by Mussa-Ivaldi et al. (1985) and Flash and Mussa-Ivaldi (1990), because they used step-like disturbances and performed the measurements at the end of the transients focussing only on the estimates of stiffness (K). On the contrary, our measurements anticipated the dynamic part of the response, and the other components ($\mathbf{B}, \mathbf{M}$) of the hand impedance can be estimated as well.

2.3 Validation of the impedance estimation method

Before estimating human hand impedance, the accuracy of the estimated impedance was analysed by applying the method to the estimation of the mass of brass weights and the spring coefficients of mechanical springs of known parameters.

For example, if the same apparatus described in the previous section is used without a subject grasping the handle, then the forces caused by the mass of the handle can be detected by the force sensor even if the robot handle moves freely: see Fig.4, where the solid and dashed lines represent measured and predicted values[2] of $dX(t)$.

Figure 5 represents correlation coefficients between measured and predicted values of the displacement $dX(t)$. Mean values and standard deviations for 6 sets of estimated results are plotted in the figure, where the horizontal axis shows the data length used for the least-squares method. The data length represents the time from the onset of the disturbance (data sampling interval is 1 ms). The correlation coefficients

[2] The prediction of $dX(t)$ was performed by numerically integrating (4) with the esitmated parameters $\hat{\mathbf{M}}, \hat{\mathbf{B}}, \hat{\mathbf{K}}$ and mesasured force $dF(t)$

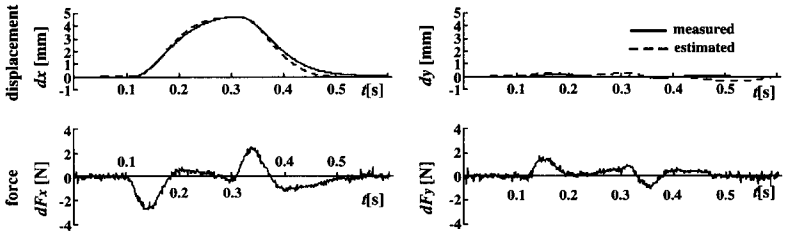

Fig. 8. Example of measured human hand displacement $dX(t)$ and force $dF(t)$ while maintaining posture, where the disturbance was applied along the direction of x-axis

increase with the length of the observation window and reach an asymptote for a window of about 450 ms. Therefore, the value of 450 ms was chosen as a standard in the following estimations.

Figure 6 shows the accuracy of estimating the inertia (i.e. mass) of brass weights (Fig.6a) and stiffness (i.e. spring coefficients) of mechanical springs (Fig.6b) attached to the robot handle. Mean values for 6 sets of estimated results are plotted, where the maximum amplitude of the disturbance is 10 mm and the data length is 450 ms. The measurement examples in Fig.4 are corresponding to the lightest case of Fig.6a. Note that only the stiffness component along the x axis of the task space is estimated in Fig.6b because of the degree of freedom of the mechanical springs used in the experiments. From Fig.6, although the inertia tends to be estimated as lower than the true value, the estimated stiffness is almost the same as its true value.

Next, in order to examine the effect of the disturbance amplitude on estimated impedance, four different values were used to estimate the stiffness of the springs. As shown in Fig.7, the estimated stiffness does not depend upon the disturbance size. However, in order to minimize the risk of voluntary responses evoked by the disturbance, the small amplitude may be preferable. Therefore, in the human experiments we used disturbances with a peak amplitude of 5 mm.

Summing up, the validity of the estimation method and experimental apparatus used in the paper was verified. In the next section, human hand impedance characteristics while maintaining posture are examined.

3 Estimated human hand impedance during maintaining posture

3.1 Experimental results

Four male subjects, 21-23 years old, performed the required task in four different locations of the workspace. Figure 8 shows an example of the measured hand displacement $dX(t)$ and force $dF(t)$, where the disturbance is applied along the direction of x-axis (see Fig.3). The measured time history of the displacement $dX(t)$ (solid lines) agrees well with the predicted value (dashed lines) which is computed by solving the differential equation (4) with estimated impedance, $\hat{\mathbf{M}}$, $\hat{\mathbf{B}}$ and $\hat{\mathbf{K}}$, and measured force $dF(t)$. This means that, under our experimental conditions, the hand dynamics of the subject is well approximated by the second-order, linear impedance model of (4).

The estimated hand impedance matrices, $\hat{\mathbf{M}}$, $\hat{\mathbf{B}}$ and $\hat{\mathbf{K}}$, for all subjects and hand locations are shown in Table 1. The estimated elements of the impedance matrices show mean values and standard deviations for 6 sets of estimated results. The arm postures of the subjects in the horizontal plane corresponding to the hand location numbers in the Table 1 are shown in Fig. 9. The conservative components of elastic force fields of the estimated stiffness matrices $\hat{\mathbf{K}}$ are larger than the non-conservative components, similar to previous results (Mussa-Ivaldi et al. 1985; Flash and Mussa-Ivaldi 1990). Also, the estimated inertia matrices $\hat{\mathbf{M}}$ and viscosity matrices $\hat{\mathbf{B}}$ are approximately symmetrical. The symmetrical components of the estimated impedance matrices are used in the following discussions by extracting the corresponding eigenvectors and eigenvalues and displaying them with an elliptical plot.

3.2 Hand inertia

Figure 9 shows inertia ellipses corresponding to the symmetrical components of the mean values of the estimated inertia matrices shown in Table 1. The inertia ellipse graphically represents the locus of the hand force vectors determined by an input disturbance consisting of an acceleration vector of unit length ($1\mathrm{m/s}^2$) rotated in all possible directions (Mussa-Ivaldi et al. 1985: Hogan 1985). The four subjects, as might be expected from the similarity of their kinematic structure, exhibit a similar pattern of hand inertia variation in different parts of the workspace: this is mainly characterized by the fact that the major axes of the ellipses tend to be aligned with the forearm, i.e. the distal part of the limb.

3.3 Hand stiffness

Figure 10 shows stiffness ellipses corresponding to the symmetrical components of the mean values of the estimated stiffness matrices shown in Table 1. The stiffness ellipse graphically represents the locus of the hand force vectors determined by an input disturbance consisting of a displacement vector of unit length (1 m) rotated in all possible directions (Mussa-Ivaldi et al. 1985).

Human hand stiffness characteristics while maintaining posture were analysed for the first time by Mussa-Ivaldi et al. (1985). In agreement with their result, our data can be characterized as follows: (1) the major axes of the stiffness ellipses tend to be oriented toward the shoulder of the subject, (2) the ellipses become more elongated as the hand location approaches the distal boundary of the work space, and (3) the ellipses become more isotropic as the hand location is moved to the proximal position. However, the sizes of our stiffness ellipses are considerably smaller than those reported in their results.

Table 1. Estimated hand impedance. Mean values and SD for 6 sets of estimated results are shown. Hand locations and arm postures of the subjects corresponding to the number in the table are shown in Fig. 9. Note that the subjects do not need to grasp the handle

Subject	Hand location	Stiffness (N/m)		Viscosity (Ns/m)		Inertia (kg)	
		Kxx	*Kxy*	*Bxx*	*Bxy*	*Mxx*	*Mxy*
		Kyx	*Kyy*	*Byx*	*Byy*	*Myx*	*Myy*
A	1	105.72 ±20.809	-104.11 ±14.757	7.17 ±0.723	-6.14 ±0.783	1.54 ±0.087	-0.57 ±0.061
		-127.35 ±31.670	234.78 ±13.913	-6.19 ±0.455	12.08 ±1.262	-0.65 ±0.034	0.94 ±0.071
	2	31.53 ± 9.810	41.36 ±12.220	3.24 ±0.382	0.81 ±0.434	0.79 ±0.034	-0.49 ±0.028
		13.83 ±13.685	380.55 ±61.946	1.18 ±1.401	22.98 ±1.541	-0.59 ±0.071	1.56 ±0.081
	3	232.77 ±12.835	-145.13 ±20.125	20.86 ±1.285	-10.69 ±1.299	1.58 ±0.086	-0.00 ±0.088
		-147.64 ± 8.169	173.38 ±19.217	-12.32 ±0.789	10.27 ±0.869	-0.10 ±0.067	0.49 ±0.104
	4	146.30 ±36.348	-63.43 ±19.104	13.17 ±1.353	-5.33 ±1.780	2.24 ±0.071	-0.51 ±0.063
		-61.26 ±21.886	98.45 ±23.219	-5.39 ±0.755	6.93 ±1.173	-0.54 ±0.134	0.71 ±0.081
B	1	81.21 ± 9.477	-93.58 ±21.478	6.36 ±0.874	-6.72 ±1.274	1.45 ±0.055	-0.63 ±0.109
		-104.59 ±30.103	208.00 ±38.658	-7.11 ±0.979	11.96 ±1.707	-0.69 ±0.125	1.13 ±0.112
	2	22.31 ± 5.863	9.51 ±13.194	2.02 ±0.188	-1.70 ±0.635	0.84 ±0.062	-0.44 ±0.053
		-1.20 ±26.476	267.25 ±26.019	-0.92 ±1.265	12.69 ±0.741	-0.53 ±0.090	1.83 ±0.084
	3	151.51 ±14.438	-123.50 ±28.834	13.00 ±2.043	-12.94 ±1.766	1.39 ±0.069	-0.27 ±0.141
		-162.12 ±18.711	213.31 ±24.622	-11.57 ±1.622	14.40 ±1.795	-0.42 ±0.071	0.73 ±0.125
	4	108.95 ±20.477	-25.78 ±14.744	15.82 ±1.402	-4.97 ±1.478	2.13 ±0.165	-0.20 ±0.111
		-42.66 ±15.085	64.10 ±11.639	-5.31 ±0.522	4.88 ±0.770	-0.39 ±0.069	0.73 ±0.039
C	1	98.82 ± 5.378	-88.20 ± 6.308	8.37 ±0.448	-6.96 ±0.444	1.48 ±0.051	-0.59 ±0.063
		-116.36 ±15.422	268.02 ±11.741	-7.21 ±0.933	16.71 ±0.994	-0.66 ±0.079	1.11 ±0.095
	2	49.63 ± 7.955	12.00 ± 9.801	4.19 ±0.441	-0.54 ±0.485	0.90 ±0.044	-0.52 ±0.065
		-7.42 ±27.734	455.50 ±31.323	0.01 ±1.327	19.90 ±0.709	-0.70 ±0.110	1.88 ±0.078
	3	257.85 ±20.088	-277.92 ±24.957	17.35 ±0.809	-16.36 ±1.311	1.82 ±0.105	-0.46 ±0.030
		-291.50 ±21.530	448.18 ±40.278	-17.77 ±1.080	22.04 ±1.742	-0.49 ±0.070	0.75 ±0.091
	4	208.43 ±19.765	-51.02 ±18.911	19.54 ±1.205	-4.28 ±0.558	2.41 ±0.099	-0.17 ±0.132
		-55.08 ± 6.179	112.22 ± 9.514	-4.61 ±0.364	5.53 ±0.368	-0.19 ±0.034	0.68 ±0.038
D	1	96.75 ±12.648	-113.56 ±12.419	8.54 ±1.054	-7.43 ±1.090	1.48 ±0.108	-0.51 ±0.063
		-110.89 ±22.398	239.86 ±51.288	-7.96 ±1.217	15.41 ±2.497	-0.50 ±0.129	0.71 ±0.099
	2	25.76 ± 8.087	29.53 ±10.030	3.15 ±0.414	0.20 ±0.395	0.75 ±0.044	-0.48 ±0.063
		16.60 ±20.994	381.84 ±24.906	1.31 ±0.600	18.46 ±1.252	-0.62 ±0.097	1.76 ±0.112
	3	114.92 ± 7.685	-85.67 ±22.312	14.90 ±0.479	-9.34 ±0.489	1.63 ±0.050	-0.16 ±0.094
		-81.59 ±11.226	107.53 ±21.847	-10.48 ±0.449	10.82 ±0.966	-0.20 ±0.035	0.46 ±0.072
	4	137.41 ±13.065	-63.42 ±16.535	13.49 ±0.479	-5.01 ±0.420	2.28 ±0.059	-0.28 ±0.073
		-77.42 ±10.742	121.64 ±13.949	-5.33 ±0.452	8.33 ±0.775	-0.36 ±0.056	0.51 ±0.028

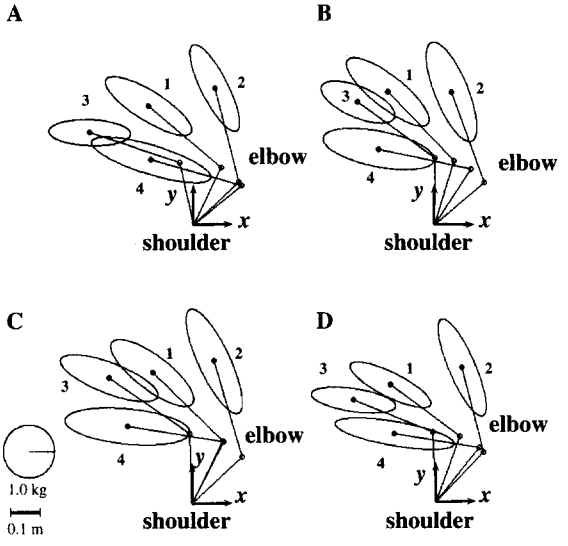

Fig. 9. Estimated inertia ellipses in several hand locations for four subjects

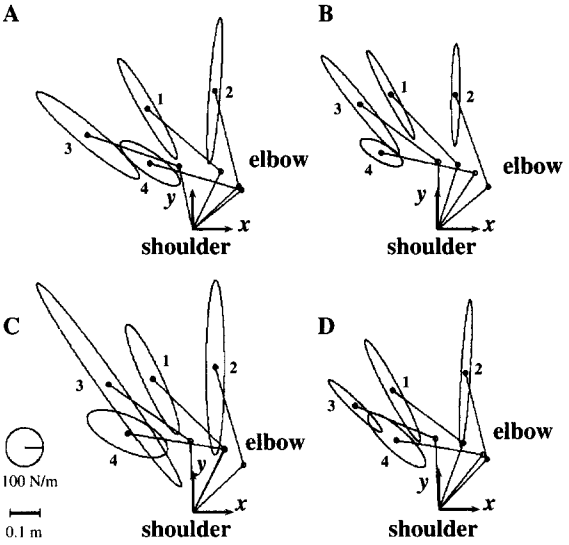

Fig. 10. Estimated stiffness ellipses in several hand locations for four subjects

3.4 Hand viscosity

Figure 11 shows viscosity ellipses related to the estimated viscosity matrices in the same way as the inertia ellipses of Fig. 9 and the stiffness ellipses of Fig. 10. The ellipse graphically represents the locus of hand force vectors responding to hand velocity vectors of unit length (1 m/s). The major and minor axes of the ellipse, respectively, show high and low viscosity in the corresponding directions. It can be seen from the figure that the major axis of the viscosity ellipse is nearly coaligned with the corresponding stiffness ellipse, i.e. it has a polar arrangement.

4 Discussion

In the present paper, human hand impedance including inertia and viscosity as well as stiffness was estimated for a multi-joint arm while maintaining posture. The symmetrical components of the estimated inertia matrices were represented by the corresponding ellipses shown in Fig. 9. As a further check, we also computed the inertia matrices from basic mechanical principles, directly measuring the lengths of the links of each subject and estimating the corresponding masses and moments of inertia according to a method proposed by Winter (1979). The estimated parameters are

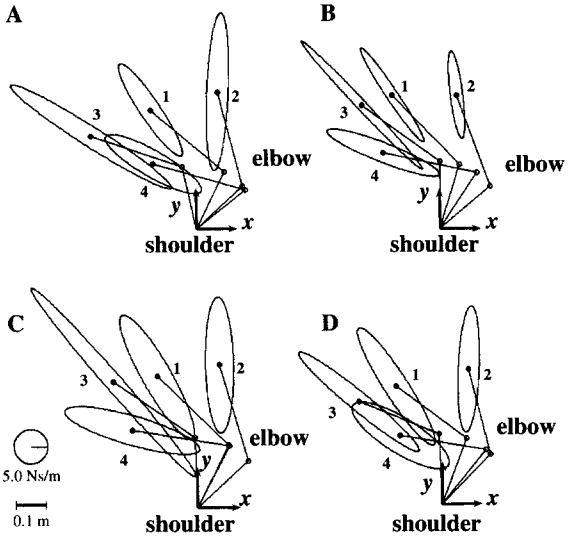

Fig. 11. Estimated viscosity ellipses in several hand locations for four subjects

Table 2. Link parameters of a two-joint arm model used in calculations of the equivalent inertia of hand motion. Inertia in the table means the moment of inertia around the centre of mass of the link

Subject	Link	Length(m)	Mass(kg)	Center of mass(m)	Inertia($\times 10^{-3}$ kg m^2)
A	Upper arm	0.21	1.68	0.09156	7.682
	Forearm + hand	0.32	1.32	0.15360	29.605
B	Upper arm	0.22	1.68	0.09592	8.431
	Forearm + hand	0.32	1.32	0.15360	29.605
C	Upper arm	0.23	1.82	0.10028	9.982
	Forearm + hand	0.33	1.43	0.15840	34.108
D	Upper-arm	0.23	1.68	0.10028	9.215
	Forearm + hand	0.29	1.32	0.13920	24.314

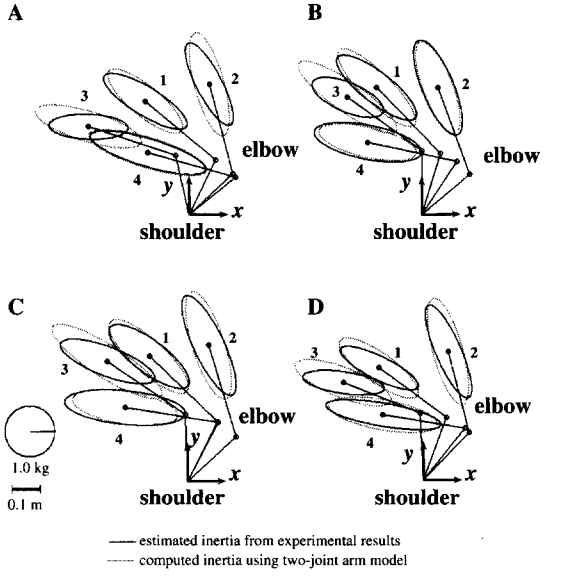

Fig. 12. Estimated and computed inertia ellipses. *dotted ellipses* show the computed equivalent inertia of the hand motion using a two-joint arm model, and *solid ellipses* are the estimated inertia from experiments

listed in Table 2, and the dotted ellipses in Fig. 12 show the computed results. Except for the ellipses at the location number 3, all other computed ellipses for different subjects and hand locations agree well with the corresponding measured ellipses. Although the differences between the estimated and computed ellipses could be analysed in detail as regards the measurement and/or approximation errors of the two-link model, it can be seen that in qualitative terms the human hand inertia characteristics in multi-joint movements can be explained from basic biomechanics.

As regards the stiffness ellipses, their spatial variation is consistent with the experimental results of Mussa-Ivaldi et al. (1985), while the sizes of our ellipses are considerably smaller than theirs, i.e. our postures were maintained with considerably less stiffness.

In particular, the joint impedance matrices corresponding to the estimated hand impedance matrices were computed using the following standard equations (Salisbury 1980).

$$\mathbf{M}_j = \mathbf{J}^T(\boldsymbol{\theta})\hat{\mathbf{M}}\mathbf{J}(\boldsymbol{\theta}) \tag{7}$$

$$\mathbf{B}_j = \mathbf{J}^T(\boldsymbol{\theta})\hat{\mathbf{B}}\mathbf{J}(\boldsymbol{\theta}) \tag{8}$$

$$\mathbf{K}_j = \mathbf{J}^T(\boldsymbol{\theta})\hat{\mathbf{K}}\mathbf{J}(\boldsymbol{\theta}) \tag{9}$$

where $\mathbf{M}_j$, $\mathbf{B}_j$ and $\mathbf{K}_j \in R^{2\times 2}$ represent joint inertia, viscosity and stiffness matrices, respectively; $\mathbf{J}(\boldsymbol{\theta}) \in R^{2\times 2}$ is the Jacobian matrix of the human arm; $\boldsymbol{\theta} = [\theta_s, \theta_e]^T \in R^2$ is the joint angle vector; and θ_s and θ_e denote shoulder and elbow joint angles, respectively (see Fig.3: θ_s is defined as the angle between the upper arm and the x-axis, and θ_e is defined as the angle between the forearm and the upper arm). Table 3 shows the joint impedance matrices for all subjects and hand locations corresponding to Table 1.

From Table 3 it can be seen that both the estimated shoulder and elbow stiffnesses range from about 4 to 13 Nm/rad. In Mussa-Ivaldi et al. (1985), the estimated shoulder and elbow stiffness ranged from about 15 to 40 Nm/rad, and Flash and Mussa-Ivaldi (1990) produced similar values. On the other hand, in single-joint arm movements, MacKay et al. (1986) found that the elbow stiffness varied from 1 to 20 (Nm/rad) depending on the joint angle. Bennett et al. (1992) showed that the range of elbow stiffness was between 3 and 15 Nm/rad and found values of elbow viscosity and inertia quite similar to the results of Table 3. The differences of the estimated impedance parameters between Mussa-Ivaldi et al. (1985) and the present paper must be critical in simulation studies such as Flash (1987) and Katayama and Kawato (1991a, b, 1993).

In order to account for the difference of scale between our stiffness estimates and those of Mussa-Ivaldi et al. (1985), we can focus on two significant aspects: the estimation procedure of hand stiffness and the physical linkage between the subject's hand and the manipulandum. While steady state data were used for stiffness estimation in Mussa-Ivaldi et al. (1985) and Flash and Mussa-Ivaldi (1990), transient data after the onset of the disturbance were used for our impedance estimation. In order to examine the differences between two methods, the steady-state data (from 0.65 to 0.8 s after the onset of the external disturbance) were used in stiffness estimation for the same subjects, with step-function disturbances in the control law of the manipulandum. Fig.13

Table 3. Joint impedance for all subjects and hand locations. Mean values and standard deviations for 6 sets of estimated results are shown. The corresponding hand impedance matrices are shown in Table 1

Subject	Hand location	Joint angle (deg)	Joint stiffness (Nm/rad)		Joint viscosity (Nms/rad)		Joint inertia (kgm^2)	
			Kss / *Kes*	*Kse* / *Kee*	*Bss* / *Bes*	*Bse* / *Bee*	*Mss* / *Mes*	*Mse* / *Mee*
A	1	θs= 62.708	7.967 ± 1.830	3.187 ± 1.075	0.651 ± 0.093	0.239 ± 0.054	0.187 ± 0.014	0.084 ± 0.008
		θe= 77.260	1.663 ± 1.974	6.901 ± 1.104	0.236 ± 0.055	0.407 ± 0.051	0.079 ± 0.010	0.060 ± 0.006
	2	θs= 41.870	6.715 ± 1.958	3.230 ± 1.286	0.723 ± 0.040	0.313 ± 0.034	0.206 ± 0.008	0.097 ± 0.006
		θe= 62.578	1.588 ± 1.386	6.819 ± 1.536	0.335 ± 0.089	0.507 ± 0.083	0.091 ± 0.003	0.059 ± 0.003
	3	θs= 102.185	11.626 ± 1.102	6.835 ± 0.750	0.748 ± 0.132	0.304 ± 0.059	0.198 ± 0.008	0.097 ± 0.006
		θe= 59.420	6.689 ± 1.250	9.383 ± 1.148	0.209 ± 0.051	0.454 ± 0.032	0.092 ± 0.008	0.059 ± 0.007
	4	θs= 37.301	4.929 ± 1.061	2.067 ± 1.263	0.421 ± 0.022	0.129 ± 0.054	0.086 ± 0.004	0.033 ± 0.006
		θe= 126.831	2.184 ± 1.103	7.090 ± 2.029	0.126 ± 0.039	0.468 ± 0.064	0.031 ± 0.010	0.056 ± 0.010
B	1	θs= 71.810	7.127 ± 2.232	2.473 ± 2.291	0.568 ± 0.084	0.141 ± 0.062	0.215 ± 0.014	0.098 ± 0.011
		θe= 62.489	1.786 ± 2.161	4.505 ± 1.705	0.117 ± 0.044	0.223 ± 0.047	0.094 ± 0.012	0.064 ± 0.007
	2	θs= 38.668	5.014 ± 1.689	1.618 ± 0.924	0.500 ± 0.075	0.113 ± 0.023	0.193 ± 0.012	0.086 ± 0.009
		θe= 71.755	0.902 ± 1.351	5.616 ± 0.981	0.165 ± 0.046	0.252 ± 0.055	0.080 ± 0.009	0.066 ± 0.006
	3	θs= 88.955	9.352 ± 1.274	4.887 ± 1.309	0.548 ± 0.144	0.026 ± 0.065	0.206 ± 0.011	0.106 ± 0.008
		θe= 55.149	2.655 ± 1.186	5.776 ± 0.674	0.105 ± 0.044	0.233 ± 0.035	0.097 ± 0.006	0.064 ± 0.003
	4	θs= 55.117	5.839 ± 1.335	3.059 ± 1.377	0.678 ± 0.071	0.102 ± 0.076	0.131 ± 0.013	0.059 ± 0.009
		θe= 112.377	1.960 ± 1.653	5.297 ± 1.426	0.080 ± 0.053	0.330 ± 0.056	0.046 ± 0.007	0.069 ± 0.004
C	1	θs= 62.512	11.252 ± 0.981	5.612 ± 0.578	1.026 ± 0.029	0.413 ± 0.038	0.221 ± 0.011	0.098 ± 0.008
		θe= 74.407	3.553 ± 1.371	9.478 ± 0.707	0.395 ± 0.051	0.626 ± 0.049	0.093 ± 0.009	0.072 ± 0.006
	2	θs= 41.467	13.387 ± 2.783	4.713 ± 1.679	1.054 ± 0.129	0.449 ± 0.084	0.252 ± 0.012	0.113 ± 0.011
		θe= 65.389	3.373 ± 0.900	9.259 ± 0.479	0.487 ± 0.068	0.584 ± 0.048	0.100 ± 0.004	0.070 ± 0.003
	3	θs= 91.277	13.252 ± 2.260	7.491 ± 1.322	0.740 ± 0.070	0.240 ± 0.061	0.260 ± 0.017	0.118 ± 0.009
		θe= 55.099	6.646 ± 2.132	13.859 ± 1.842	0.152 ± 0.061	0.530 ± 0.061	0.116 ± 0.009	0.070 ± 0.006
	4	θs= 61.714	12.854 ± 0.869	5.812 ± 0.995	1.028 ± 0.049	0.239 ± 0.047	0.167 ± 0.009	0.063 ± 0.009
		θe= 109.379	5.522 ± 0.411	10.705 ± 0.738	0.216 ± 0.039	0.490 ± 0.042	0.062 ± 0.003	0.073 ± 0.003
D	1	θs= 68.879	6.757 ± 1.188	1.761 ± 1.308	0.722 ± 0.059	0.232 ± 0.049	0.176 ± 0.020	0.064 ± 0.011
		θe= 75.090	1.933 ± 1.965	7.028 ± 2.486	0.198 ± 0.068	0.480 ± 0.105	0.064 ± 0.013	0.042 ± 0.005
	2	θs= 44.259	6.364 ± 0.765	1.157 ± 0.779	0.707 ± 0.057	0.239 ± 0.047	0.205 ± 0.006	0.082 ± 0.006
		θe= 60.308	0.408 ± 1.644	5.005 ± 1.098	0.303 ± 0.077	0.377 ± 0.038	0.073 ± 0.008	0.046 ± 0.005
	3	θs= 91.938	5.739 ± 1.128	1.975 ± 1.124	0.680 ± 0.046	0.188 ± 0.049	0.188 ± 0.008	0.073 ± 0.007
		θe= 66.033	2.224 ± 1.839	4.240 ± 1.325	0.119 ± 0.056	0.379 ± 0.058	0.071 ± 0.005	0.042 ± 0.004
	4	θs= 49.920	4.851 ± 1.119	1.699 ± 1.055	0.515 ± 0.026	0.117 ± 0.018	0.104 ± 0.004	0.024 ± 0.005
		θe= 120.577	0.895 ± 0.616	8.337 ± 0.981	0.099 ± 0.046	0.571 ± 0.061	0.019 ± 0.004	0.038 ± 0.003

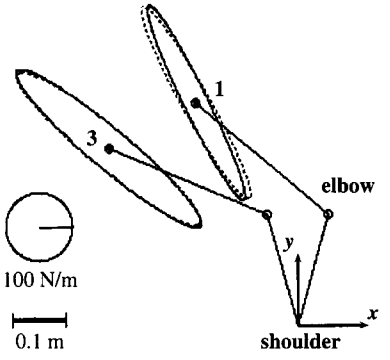

Fig. 13. Comparison between dynamic and static estimations for the same subject, where the *solid* and *dotted lines* indicate the stiffness ellipses estimated from the transient data (0.45 s of the data length) and the steady state data (from 0.65 to 0.8 s after the onset of the external disturbance), respectively

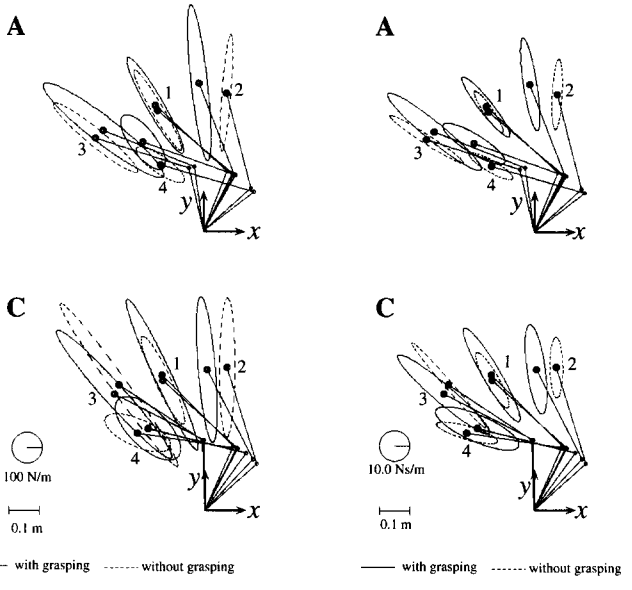

(a) Hand stiffness (b) Hand viscosity

Fig. 14a,b. The effects of grasping the handle on the estimated stiffness and viscosity ellipses. The *solid* and *dashed ellipses* show the estimated impedance with and without grasping and correspond to the symmetrical components of the mean values of the estimated matrices shown in Tables 4 and 1, respectively. **a** Hand stiffness. **b** Hand viscosity

shows estimated results for the same subject, where the solid and dotted lines indicate the stiffness ellipses estimated from the transient and steady-state data, respectively. Evidently, the two computational procedures yield the same results.

Thus, we focussed our attention on the hand-manipulandum linkage. While the subjects in the setup of Mussa-Ivaldi et al. (1985) were required to grasp the handle, our subjects did not need to do so since the molded plastic cast fixing the wrist and the hand was tightly attached to the robot handle. In order to examine the difference, another plastic cast was used in the experiments. The plastic cast fixed the wrist joint of the subject in order to avoid any motion, but the hand was left free, and so the subjects had to grasp the handle in order to keep the hand location. Table 4 shows the estimated hand impedance ($\hat{\mathbf{M}}, \hat{\mathbf{B}}, \hat{\mathbf{K}}$), i.e. mean values and SD of each matrix element for 6 sets of experimental data. Figure 14 shows the results in a graphical way, plotting the stiffness and viscosity ellipses in the two cases. The solid

Table 4. Estimated hand impedance while the subjects grasped the handle in order to keep the hand location. Mean values and standard deviations for 6 sets of estimated results are shown. Hand locations and arm postures of the subjects are shown in Fig. 14

Subject	Hand location	Stiffness (N/m)		Viscosity (Ns/m)		Inertia (kg)	
		K_{xx}	K_{xy}	B_{xx}	B_{xy}	M_{xx}	M_{xy}
		K_{yx}	K_{yy}	B_{yx}	B_{yy}	M_{yx}	M_{yy}
A	1	130.51 ± 12.414	-123.18 ± 10.629	12.20 ± 1.005	-9.68 ± 1.146	1.22 ± 0.109	-0.31 ± 0.079
		-140.79 ± 17.825	283.35 ± 28.047	-10.08 ± 1.081	16.85 ± 2.207	-0.28 ± 0.080	0.57 ± 0.160
	2	58.26 ± 8.300	-45.581 ± 8.589	5.03 ± 0.800	-4.13 ± 0.653	0.96 ± 0.052	-0.57 ± 0.056
		-54.01 ± 14.490	506.08 ± 44.022	-3.99 ± 0.494	30.02 ± 2.961	-0.55 ± 0.068	0.98 ± 0.199
	3	340.48 ± 8.277	-201.33 ± 22.160	26.03 ± 0.790	-14.55 ± 1.481	1.26 ± 0.107	0.07 ± 0.108
		-193.63 ± 21.492	237.26 ± 25.171	-18.19 ± 1.055	19.32 ± 1.059	0.09 ± 0.070	0.32 ± 0.038
	4	132.01 ± 30.636	-67.69 ± 11.074	18.83 ± 1.739	-7.26 ± 0.591	1.37 ± 0.131	-0.24 ± 0.050
		-59.95 ± 14.613	166.70 ± 17.981	-8.25 ± 0.456	10.84 ± 0.933	-0.20 ± 0.053	0.54 ± 0.043
C	1	142.98 ± 22.524	-160.48 ± 6.313	13.37 ± 0.398	-13.52 ± 0.609	1.35 ± 0.041	-0.35 ± 0.029
		-213.02 ± 15.644	454.83 ± 36.677	-12.50 ± 0.917	27.69 ± 1.266	-0.44 ± 0.074	0.74 ± 0.070
	2	58.52 ± 8.265	-24.16 ± 9.430	6.45 ± 0.232	-3.80 ± 0.573	1.08 ± 0.054	-0.58 ± 0.021
		-44.96 ± 20.305	474.26 ± 26.464	-2.80 ± 1.476	29.09 ± 1.229	-0.64 ± 0.089	1.18 ± 0.089
	3	287.01 ± 11.951	-229.36 ± 26.983	25.29 ± 1.916	-15.80 ± 1.226	1.43 ± 0.083	-0.09 ± 0.080
		-259.03 ± 18.366	338.17 ± 27.906	-17.06 ± 1.165	19.91 ± 1.276	-0.10 ± 0.015	0.50 ± 0.049
	4	200.00 ± 38.055	-60.59 ± 18.146	26.22 ± 1.698	-7.12 ± 0.655	1.85 ± 0.071	-0.19 ± 0.099
		-85.45 ± 25.739	193.41 ± 24.567	-8.09 ± 0.539	11.93 ± 0.769	-0.32 ± 0.095	0.55 ± 0.057

Table 5. Geometrical parameters of estimated stiffness and viscosity ellipses in Figs. 10 and 11, where the subjects did not need to grasp the handle. The size of the ellipse is defined by the area of the ellipse, and the orientation is defined by a counterclockwise angle from the x-axis of the task coordinate system to the major axis of the ellipse. Also, the shape of the ellipses is defined by the ratio between the lengths of the major and minor axes. Mean values and standard deviations for 6 sets of estimated results are shown

Subject	Hand location	Stiffness ellipses			Viscosity ellipses		
		Size ($\times 10^4$ (N/m)^2)	Orientation (deg)	Shape (dimensionless)	Size$_2$ ((Ns/m)^2)	Orientation (deg)	Shape (dimensionless)
A	1	3.51 ± 0.92	120.04 ± 3.22	8.89 ± 2.82	150.83 ± 24.37	124.29 ± 3.00	5.65 ± 1.02
	2	3.65 ± 1.54	85.50 ± 1.08	14.26 ± 4.02	229.21 ± 30.51	87.20 ± 2.37	7.37 ± 0.75
	3	5.90 ± 0.70	140.83 ± 2.34	6.70 ± 0.74	255.91 ± 40.74	147.42 ± 1.89	10.00 ± 1.32
	4	3.36 ± 1.44	144.35 ± 5.15	3.74 ± 1.22	195.93 ± 36.76	150.44 ± 2.76	4.28 ± 0.55
B	1	2.16 ± 1.14	118.66 ± 2.23	13.33 ± 7.80	86.98 ± 20.13	123.96 ± 2.30	10.43 ± 2.49
	2	1.74 ± 0.48	88.97 ± 4.40	14.75 ± 6.68	72.27 ± 8.64	97.01 ± 4.75	7.37 ± 0.97
	3	3.68 ± 0.44	128.94 ± 2.31	9.44 ± 2.26	117.54 ± 43.68	133.32 ± 1.34	19.87 ± 6.23
	4	1.76 ± 0.60	151.03 ± 5.70	3.65 ± 2.75	158.42 ± 32.81	158.57 ± 2.69	6.54 ± 1.11
C	1	5.03 ± 0.59	115.19 ± 0.88	6.31 ± 0.71	280.71 ± 21.69	119.73 ± 1.68	4.85 ± 0.38
	2	7.08 ± 1.45	89.64 ± 2.06	9.50 ± 1.30	260.21 ± 30.61	90.99 ± 2.54	4.85 ± 0.50
	3	10.91 ± 2.59	125.77 ± 0.83	12.74 ± 2.07	287.10 ± 48.34	131.12 ± 0.56	15.24 ± 2.35
	4	6.47 ± 0.93	156.35 ± 2.48	2.63 ± 0.26	276.31 ± 22.92	163.80 ± 0.96	4.98 ± 0.70
D	1	3.15 ± 0.84	119.32 ± 5.04	9.58 ± 2.29	221.57 ± 35.45	123.15 ± 4.58	6.04 ± 0.94
	2	2.83 ± 0.69	86.18 ± 2.43	17.57 ± 5.15	179.18 ± 15.00	87.11 ± 1.32	6.09 ± 0.99
	3	1.62 ± 0.46	136.47 ± 4.62	8.16 ± 2.72	196.84 ± 28.25	140.82 ± 1.85	8.60 ± 1.18
	4	3.67 ± 0.96	138.65 ± 3.45	3.74 ± 1.30	268.77 ± 32.24	148.22 ± 2.19	3.29 ± 0.30

and dashed ellipses show the estimated impedance with and without grasping and correspond to the symmetrical components of the mean values of the estimated matrices shown in Tables 4 and 1, respectively.

In order to give a more intuitive interpretation of the difference between the two cases, the impedance data in Tables 1 and 4 were transformed in an equivalent representation based on three parameters of each impedance ellipse: (1) the size (defined by the ellipse area), (2) the orientation (defined by the counterclockwise angle from the x-axis of the task coordinate system to the major axis of the ellipse), (3) the shape (defined by the ratio between the lengths of the major and minor axes). Thus, Table 1 is transformed in Table 5 and Table 4 into Table 6.

Comparing Table 5 with Table 6, it can be seen that the sizes of both the stiffness and viscosity ellipses are increased by grasping the handle. Milner (1993) found that greater voluntary muscle activation was responsible for lower joint compliance. Therefore, a likely explanation for the increase of the sizes of the ellipses comes from the voluntary muscle activation caused by grip forces in order to grasp the handle, since there are some multi-joint muscles which act on both the hand and elbow movements, as pointed out by Gomi et al. (1992a) and Katayama and Kawato (1993).

As regards the estimated hand viscosity, the major axis of the viscosity ellipse was nearly parallel to the one of the corresponding stiffness ellipse. From Table 5 it can be seen in different subjects and hand locations that the orientations of the viscosity ellipses are almost the same as those of the stiffness ellipses, and that the viscosity ellipses become more isotropic as the hand location approaches the proximal position, similar to the stiffness ellipses. Also, in Table 6 where the sizes of the ellipses are larger than in Table 5 because of the grip force, these findings are also true.

Flash and Mussa-Ivaldi (1990) showed that the spatial variations of the hand stiffness ellipses in the horizontal plane could be explained by a covariation between the shoulder stiffness and the stiffness component provided by two-joint muscles. Viscoelastic properties of skeletal muscles are transmitted to the hand motion through the kinematics of the musculoskeletal system of the arm. As a result, the spatial variations of the viscosity ellipses shown in this paper may be explained by the coordinated activities between the single-joint muscles about the shoulder joint and the two-joint muscles acting on both the shoulder and elbow joints.

The finding that the hand viscosity ellipses are approximately parallel to the hand stiffness ellipses is quite important from a control point of view. If the hand viscosity were fully isotropic or orthogonal to the hand stiffness, the dynamic behaviour of the hand motion would have different damping characteristics in different movement directions, which obviously is a quite undesirable feature. Although the hand inertia characteristics should be taken into account, the isotropic dynamic behaviour of the hand motion could be

Table 6. Geometrical parameters of estimated stiffness and viscosity ellipses while the subjects grasped the handle in order to keep the hand location. Mean values and standard deviations for 6 sets of estimated results are shown

Subject	Hand location	Stiffness ellipses			Viscosity ellipses		
		Size ($\times 10^4$ (N/m)^2)	Orientation (deg)	Shape (dimensionless)	Size ((Ns/m)^2)	Orientation (deg)	Shape (dimensionless)
A	1	6.20 ±1.35	120.00 ± 0.96	6.70 ±0.72	341.12 ± 73.43	128.49 ±1.94	5.71 ±0.44
	2	8.50 ±1.97	96.27 ± 1.02	10.01 ±1.83	426.80 ±103.77	99.05 ±1.02	7.18 ±1.11
	3	13.03 ±1.27	142.48 ± 2.41	5.92 ±0.58	736.58 ± 82.94	140.81 ±0.72	6.71 ±0.93
	4	5.75 ±1.93	127.13 ± 4.45	2.66 ±0.23	449.51 ± 48.08	148.53 ±3.67	3.92 ±0.07
C	1	9.31 ±2.69	115.22 ± 2.50	11.06 ±3.94	630.42 ± 56.66	120.58 ±1.41	6.29 ±0.55
	2	8.36 ±1.80	94.77 ± 1.76	8.81 ±1.03	552.79 ± 46.23	98.12 ±2.26	4.99 ±0.29
	3	11.64 ±2.43	132.10 ± 1.34	8.93 ±2.68	726.95 ± 63.38	139.57 ±2.03	6.75 ±1.05
	4	10.60 ±3.01	135.83 ± 3.96	2.21 ±0.31	803.98 ±107.36	156.60 ±0.38	3.43 ±0.19

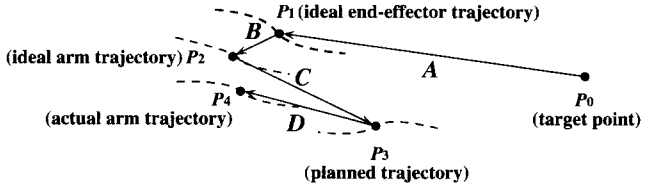

Fig. 15. Five different representations of the time-varying end-effector point ($P_0 - P_4$), linked by four neuro-muscular processes ($A - D$)

preserved by the parallel relation between the hand stiffness and viscosity ellipse.

In the more general context of motor planning and control, we think that the critical role of the human hand (or end-effector) impedance can be understood by distinguishing five different representations of the time-varying end-effector point ($P_0 - P_4$), linked by four neuromuscular processes ($A - D$) as sketched in Fig.15.

- P_0 is the *target point*, typically fixed during simple reaching movements.
- P_1 is the *ideal moving target*, internally generated by some process A. The literature proposes static models like the *minimum jerk model* (Flash and Hogan 1985) or dynamic models like VITE (Bullock and Grossberg 1989) or the ξ-model (Morasso et al. 1993).
- P_2 expands the previous representation by computing the global arm/body configuration and this includes a task-dependent selection/optimization process B required to solve the motor redundancy problem (see Morasso and Sanguineti 1992 for a model based on self-organized networks).
- P_3 is the planned equilibrium point at each time instant, coherently with the elastic properties of muscles. In some models (Flash 1987), P_3 coincides with P_2, in the hope that motor impedance keeps to an acceptable level the effects of mechanical dynamics. In other models, P_3 is computed by an additional process C (Katayama and Kawato 1991a) which approximately inverses the hand impedance.
- P_4 is the actual trajectory which differs from P_3 for the constraining effects of the arm impedance and mechanical arm dynamics (physical process D). Except in pathological situations, P_1, P_2, P_4 should be very close, whereas P_3 might lead or lag according to specific dynamic conditions.

P_1, P_2, P_3 are *hidden units* from the point of view of experimental behavioural observations. Neurophysiology might help, but the task of distinguishing them is certainly an open question worth investigating. In any case, it is necessary to keep in mind this kind of multi-representation arrangement in order to grasp the flexibility of the system.

Finally, the main results of our experiments can be summarized as follows: (1) the estimated inertia matrices of the human hand agreed well with computed values using a two-joint arm model, (2) spatial variations of the stiffness ellipses are approximately the same as the experimental results of Mussa-Ivaldi et al. (1985), (3) the grip force of the subject increases the hand stiffness and viscosity, and (4) the orientations of viscosity ellipses are almost parallel to those of the stiffness ellipses.

Further research will be directed to clarifying changes of the human hand impedance depending on the activation level of the muscles, task instruction to the subjects, and 3D arm postures.

Acknowledgement. We are grateful to Drs. F.A.Mussa-Ivaldi, V.Sanguineti and M.Nagamachi for their helpful comments and discussions. The work was supported in part by Nissan Research Foundation to T.Tsuji.

References

1. Asada H, Slotine JJ (1986) Robot analysis and control. Wiley, New York
2. Bennett DJ, Hollerbach JM, Xu Y, Hunter IW (1992) Time varying stiffness of human elbow joint during cyclic voluntary movement. Exp Brain Res 88: 433-442
3. Bizzi E, Accornero N, Chapple W, Hogan N (1984) Posture control and trajectory formation during arm movement. J Neurosci 4: 2738-2744
4. Bullock D, Grossberg (1989) S VITE and FLETE: neural modules for trajectory formation and postural control. In: Hershberger W (ed) Volitional action. North-Holland, Amsterdam, pp 253-297
5. Cannon S, Zahalak GI (1982) The mechanical behavior of active human skeletal muscles in small oscillations. J Biomech 15: 111-121
6. Dolan JM, Friedman MB, Nagurka ML (1993) Dynamic and loaded impedance components in the maintenance of human arm posture. IEEE Trans Syst Man Cybern 23: 698-709
7. Flash T (1987) The control of hand equilibrium trajectories in multi-joint arm movement. Biol Cybern 57: 257-274
8. Flash T, Hogan N (1985) The coordination of arm movements: an experimentally confirmed mathematical model. J Neurosci 5: 1688-1703
9. Flash T, Mussa-Ivaldi FA (1990) Human arm stiffness characteristics during maintenance of posture. Exp Brain Res 82: 315-326
10. Gomi H, Koike Y, Kawato M (1992a) Measurement of the stiffness during multi-joint arm movement. Technical report of Institute of Electronics, Information and Communication Engineers NC91-145: 99-106 (in Japanese)

11. Gomi H, Koike Y, Kawato M (1992b) Human hand stiffness during discrete point-to-point multi- joint movement. Proceedings of the Annual International Conference of the IEEE Engineering in Medicine and Biology Society, pp 1628-1629
12. Hogan N (1984) An organizing principle for a class of voluntary movements. J Neurosci 4: 2745-2754
13. Hogan N (1985) The mechanics of multi-joint posture and movement control. Biol Cybern 53: 1-17
14. Katayama M, Kawato M (1991a) Parallel-hierarchical neural network model for motor control of musculoskeletal system. Systems and Computers in Japan, Scripta Technica Inc 22: 95- 105
15. Katayama M, Kawato M (1991b) Virtual trajectory and stiffness ellipse during force-trajectory control using a parallel-hierarchical neural network model. Fifth International Conference on Advanced Robotics, pp 1187-1194
16. Katayama M, Kawato M (1993) Virtual trajectory and stiffness ellipse during multi-joint arm movement predicted by neural inverse models. Biol Cybern 69: 353-362
17. Kawato M, Furukawa K, Suzuki R (1987) A hierarchical neural-network model for control and learning of voluntary movement. Biol Cybern 57: 169-185
18. Lacquaniti F, Licata F, Soechting JF (1982) The mechanical behavior of the human forearm in response to transient perturbations. Biol Cybern 44: 35-46
19. MacKay WA, Crammond DJ, Kwan HC, Murphy JT (1986) Measurements of human forearm viscoelasticity. J Biomech 19: 231-238
20. Milner TE (1993) Dependence of elbow viscoelastic behavior on speed and loading in voluntary movements. Exp Brain Res 93: 177-180
21. Morasso P, Sanguineti V (1992) SOBoS - a self-organizing body schema. In: Aleksander I, Taylor J (eds) Artificial neural networks. North-Holland, Amsterdam, pp 487-490
22. Morasso P, Sanguineti V, Tsuji T (1993) A model for the generation of target signals in trajectory formation. Sixth International Conference on Handwriting and Drawing, pp 74-76
23. Mussa-Ivaldi FA, Hogan N, Bizzi E (1985) Neural, mechanical and geometrical factors subserving arm posture in humans. J Neurosci 5: 2732-2743
24. Paul R (1981) Robot manipulators; mathematics, programming, and control. MIT Press, Cambridge, Mass.
25. Salisbury JK (1980) Active stiffness control of a manipulator in Cartesian Coordinates, Proceedings of IEEE Conference on Decision and Control, pp 95-100
26. Winter DA (1979) Biomechanics of human movement. Wiley-Interscience, New York